Yancheng Wang
State Key Lab of Fluid Power Transmission and Control,
Department of Mechanical Engineering,
Zhejiang University,
Hangzhou 310027, China
e-mail: yanchwang@zju.edu.cn

Roland K. Chen
Mem. ASME
Mechanical Engineering,
University of Michigan,
1043E HH Dow, 2300 Hayward St.,
Ann Arbor, MI 48109
e-mail: krchen@umich.edu

Bruce L. Tai
Mem. ASME
Mechanical Engineering,
University of Michigan,
1043A HH Dow, 2300 Hayward St.,
Ann Arbor, MI 48109
e-mail: krchen@umich.edu

Kai Xu
UM-SJTU Joint Institute,
Shanghai Jiao Tong University,
Shanghai 200240, China
e-mail: k.xu@sjtu.edu.cn

Albert J. Shih
Fellow ASME
Mechanical Engineering
and Biomedical Engineering,
University of Michigan,
3001E EECS, 2350 Hayward St.,
Ann Arbor, MI 48109
e-mail: shiha@umich.edu

Study of Insertion Force and Deformation for Suturing With Precurved NiTi Guidewire

This research presents an experimental study evaluating stomach suturing using a precurved nickel–titanium (NiTi) guidewire for an endoscopic minimally invasive obesity treatment. Precise path planning is critical for accurate and effective suturing. A position measurement system utilizing a hand-held magnetic sensor was used to measure the shape of a precurved guidewire and to determine the radius of curvature before and after suturing. Ex vivo stomach suturing experiments using four different guidewire tip designs varying the radius of curvature and bevel angles were conducted. The changes in radius of curvature and suturing force during suturing were measured. A model was developed to predict the guidewire radius of curvature based on the measured suturing force. Results show that a small bevel angle and a large radius of curvature reduce the suturing force and the combination of small bevel angle and small radius of curvature can maintain the shape of guidewire for accurate suturing. [DOI: 10.1115/1.4029311]

Keywords: suturing, precurved guidewire, insertion force, stomach

1 Introduction

Suturing during minimally invasive surgery remains a challenging and a time-consuming task, even with the assistance of robotic surgical systems, due to the limited dexterity allowed in the space of operation [1]. Minimally invasive surgery, such as endoscopic or laparoscopic surgery, is less traumatic to patients and enables better postoperative recovery. However, the increased suturing time may increase the risk of infection and other complications [2]. Therefore, enhancing suturing efficiently is critical to reduce infections, complications, and overall procedure times [3].

A novel method utilizing a precurved super-elastic nickel–titanium (NiTi) guidewire to perform endoscopic suturing inside the stomach has been developed by Xu et al. [4]. During this suturing procedure, the guidewire penetrates outside the stomach. To avoid injury to the organs surrounding the stomach, the trajectory of the guidewire insertion, which is closely related to its radius of curvature, must be accurate and predictable. However, the guidewire is deformed due to the insertion force [5]. Experimental studies [6] and modeling of needle–tissue interaction forces [7–9] of the needle have been presented, but limited research has been conducted on compliant, precurved NiTi guidewires. Okazawa et al. analyzed the deflection of a precurved needle stylet within a cannula, but the insertion force was not studied [10]. The goal of this study is to measure the force and radius of curvature while suturing a stomach using the precurved NiTi guidewire. Furthermore, we developed a mathematical model to predict the guidewire radius of curvature based on the measured insertion force.

Accurate measurement of soft and/or compliant objects is technically challenging. Optical methods (e.g., stereo camera and X-ray) have been utilized to reconstruct the deformed needle geometries and insertion paths [9,11,12]. These optical methods usually require intensive images processing and system registration. Alternatively, the haptic position measurement system (HPMS) has been developed for contact measurement of soft and/or flexible objects [13]. This system utilizes an electromagnetic tracking (EMT) system to detect and record 3D position and orientation of the magnetic sensor that touches the soft and flexible object and is secured at the tip of a hand-held needle cannula. Figure 1 shows a HPMS consisting of a transmitter, magnetic sensor, needle cannula, and electronic unit. The transmitter has three coils oriented orthogonally and emitting a magnetic field to be received by the magnetic sensor. The magnetic sensor also consists of coils, which receive the magnetic field and generate a current signal. The electronic unit synchronizes the transmitter and sensor signals and calculates the position and orientation of the sensor [14]. The sensor is guided by the user's hand to determine the contact position by coordinating vision and haptic sensations.

Manuscript received July 7, 2014; final manuscript received November 20, 2014; published online February 5, 2015. Assoc. Editor: Pasquale Vena.

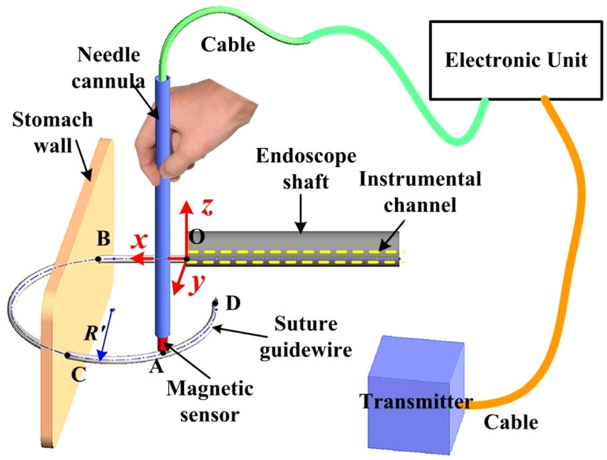

Fig. 1 Schematic view of the precurved NiTi guidewire for endoscopic suturing of stomach and an overview of the HPMS, including a magnetic sensor in a needle cannula touching the guidewire for measurement

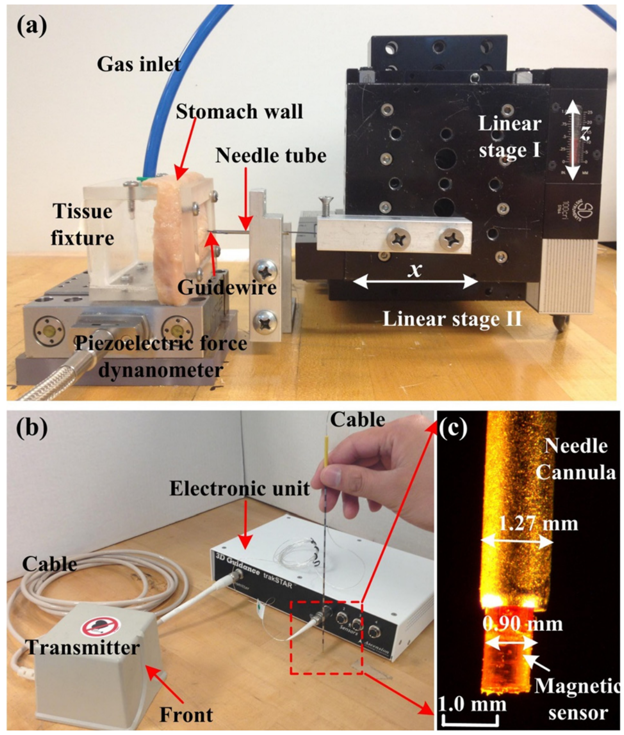

Fig. 2 Experimental setup for precurved guidewire insertion into stomach: (*a*) overview setup, (*b*) HPMS, and (*c*) microscopic view of the magnetic sensor protruding outside the tip of a needle cannula

When the hand-held magnetic sensor is touching or close to the subject, the user determines the location to record the position and orientation of the magnetic sensor as a measurement point. This research utilizes the HPMS to measure the shape of a precurved NiTi guidewire.

In this paper, a precurved guidewire suturing experiment setup and procedure are described. This is followed by guidewire suturing in ex vivo porcine stomach and the measurement of the insertion force and radius of curvature of guidewire using the proposed HPMS. A model to predict the radius of curvature based on the measured force is developed and validated.

2 Methods

2.1 Precurved Guidewire Suturing Experiment Setup. Figure 2(*a*) shows an overview of the experimental setup to study a precurved NiTi guidewire suturing of an ex vivo porcine stomach. The precurved guidewire was straightened by pulling it through a straight needle tube (1.27 mm outside diameter, 1.04 mm inside diameter, and 35 mm long). Three linear stages (Siskiyou instruments 200cri) with 1 μm resolution were assembled to align and insert the guidewire into the stomach, which was constrained to one side in an acrylic tissue fixture. Experiments were carried out ex vivo on porcine stomach wall which were freshly preserved and cut into the size of approximately 6 mm thick and 50 mm $\times$ 40 mm in area. The stomach wall consists of the mucosa (inner layer) and muscularis mucosae (outer layer) [15]. An air pressure of 5.0 kPa was applied to the tissue fixture to inflate the stomach wall for insertion test. A Kistler 9256C piezoelectric force dynamometer underneath the stomach chamber (tissue fixture in Fig. 2(*a*)) was used to measure the insertion force, which can be decomposed into the x- and y-direction components, marked as F_x and F_y, respectively, during guidewire suturing. For all tests, the guidewire insertion speed was set at 1.5 mm/s. Three repeated suturing tests were conducted for each guidewire.

To measure the shape of the guidewire before and after suturing, HPMS was utilized. Figure 2(*b*) shows the setup of HPMS, which consists of a miniature (0.90 mm outer diameter) magnetic sensor (Ascension Model 90), as shown in Fig. 2(*c*). A thin cable connects the sensor to the electronic unit. The sensor was fixed inside the tip of an 18-gauge stainless steel needle cannula (Figs. 2(*b*) and 2(*c*)). The tip of the sensor was exposed from the needle tip and used as a touch probe. The DC EMT with front transmitter orientation and sampling time of 0.5 s has the accuracy and capability of measuring position with 0.2 mm resolution [16]. The position of the magnetic sensor was recorded at the contact point on the guidewire. By collecting several points along the guidewire, the shape of the curved guidewire could be determined.

2.2 Precurved Guidewire Design and Fabrication. The NiTi guidewire was 0.69 mm in diameter and consisted of 55 wt.% of Ni and 45 wt.% of Ti. The superelasticity property NiTi alloy has a high elastic strain limit (up to 8%) [17]. The five-step procedure of precurved guidewire fabrication and suturing experiment is illustrated in Fig. 3. In step 1, the tip of the guidewire with three symmetric planes of either a bevel angle of 5 deg or 10 deg is sharpened by surface grinding using the setup and procedure presented by Wang et al. [18]. In step 2, the guidewire is curved into an aluminum die with a circular groove machined to hold the guidewire for heat treatment (0.5 h at 550 °C, then oil-quenched to room temperature). After heat treatment, the guidewire maintains its curved shape. In step 3, the guidewire is straightened by pulling it through a needle tube (1.27 mm diameter and 35 mm long). This tube and guidewire assembly is delivered via the instrument channel of an endoscope to touch the stomach wall, as shown in step 4. In step 5, the guidewire is pushed outward from the tube and curved to penetrate through the stomach to create a suture.

Four precurved guidewires, marked as wires I, II, III, and IV, with 6.9 mm (wires I and II) and 8.6 mm (wires III and IV) radii of curvature were designed and tested. The corresponding elastic strain of the guidewire in the groove inside the heat-treatment die was 4% and 5%, respectively. Wires I and III had a sharp 5 deg bevel angle (as shown in the top of step 1 in Fig. 3) while wires II and IV had a 10 deg bevel angle. Due to springback after heat treatment, the radius of curvature of the guidewire was slightly larger than that of the die. The radius of curvature for the final fabricated guidewires was measured by an electronic micrometer (Mitutoyo Model 293-831) as 7.61 mm, 7.93 mm, 9.27 mm, and 8.96 mm for wires I, II, III, and IV, respectively.

2.3 Precurved Guidewire Shape Measurement. In this study, the HPMS was utilized to measure the suturing path and radius of curvature of the guidewire. The sensor was guided by hand and perpendicularly touched point A on the guidewire along the central line (as in Fig. 1), and the haptic feedback was used to determine the contact position between the sensor and guidewire. As shown in Fig. 1, a Cartesian coordinate system was defined based on the needle cannula. The origin (O) was defined on the guidewire which contacting with the needle cannula and the x-axis is along the needle cannula (Fig. 2(*a*)). The curved guidewire was generally in the x–y plane. During the experiment, four points (Fig. 1) were selected to be touched and measured: (1) the origin of the xyz coordinate system (O), (2) the point where the guidewire penetrated into stomach (B), (3) the point where the guidewire penetrated out of the stomach (C), and (4) the end position of the guidewire tip (D). For each point position measurement, the sensor touched the target point for 1 s while the electronic unit recorded the positional data. The least square fitting method was applied to fit a circle through these four points and find the radius of curvature to represent the shape of the guidewire.

Wires I and III were first measured by advancing the guidewire 30 and 35 mm, respectively, out of the needle tube without touching stomach. During this time, a micrometer was used to measure the radius of curvature of the guidewire as the datum. The HPMS was used to measure the four points, and the data were used to fit a circular arc to calculate the undeformed radius of curvature of the guidewire and study the accuracy of the radius of curvature measurement. Then, four points (O, B, C, and D) on the guidewire after suturing the stomach were measured using the HPMS. The change in radius of curvature of wires I–IV was calculated to quantify the effects of bevel angle (sharpness) and initial radius of curvature. All measurements were taken with the magnetic sensor touching the guidewire in the z direction, as shown in Fig. 1.

2.4 Analytical Model Prediction of the Guidewire Radius of Curvature. To predict the guidewire radius of curvature, an analytical model was developed based on the measured insertion forces. Figure 4(*c*) shows a precurved guidewire before (marked as datum OGEC) and after penetrating out of the stomach at point C (as shown in Fig. 1). Point O was the origin of the xy coordinate system. The datum guidewire was assumed to be a circular arc with a radius of curvature of R and centered at O′ (0, R). The guidewire was subjected to a total force of (F_E^x and F_E^y), uniformly distributed along the arc CG at the tip. After penetrating out of the stomach, this force was released and the guidewire sprung back to a circular arc $OG_1E_1C_1$ with the radius of curvature R_1 and the center at point O_1. The length of arc CG ($l_{\widehat{CG}}$) was assumed to be 6 mm the thickness of stomach wall. The resultant forces in x- and

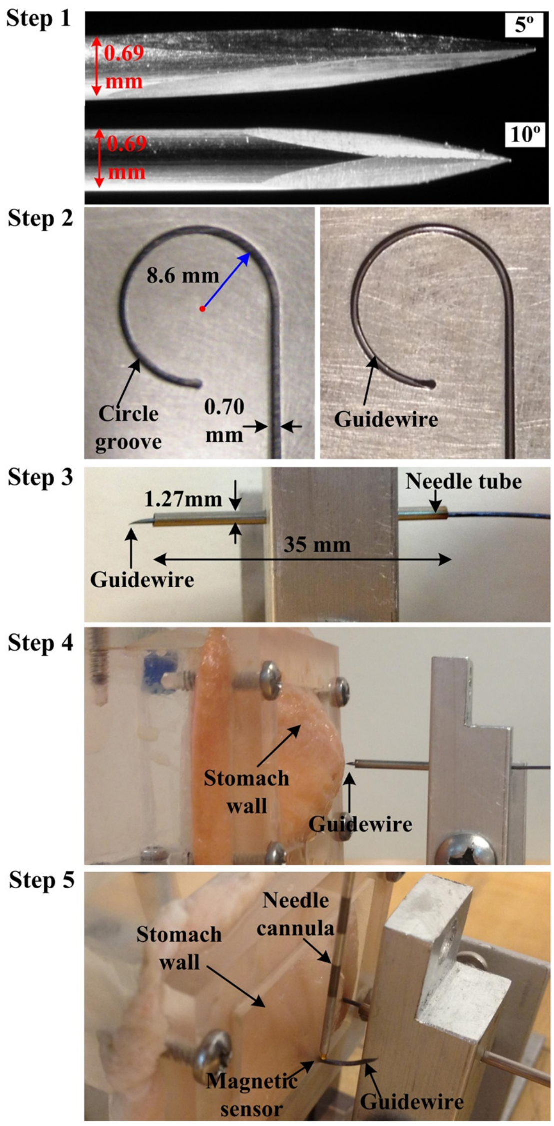

Fig. 3 Five steps of precurved guidewire fabrication and suturing

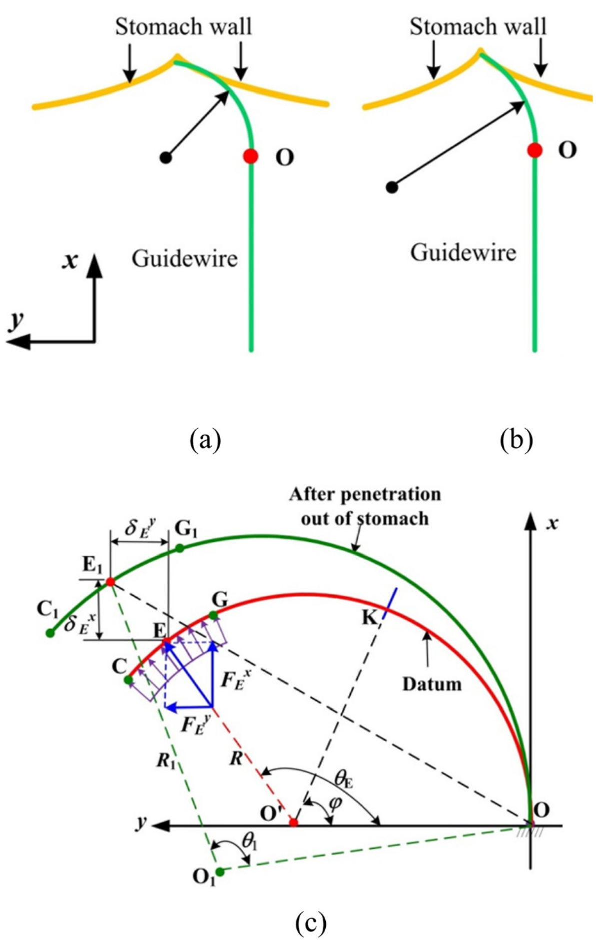

Fig. 4 Schematic view of guidewire penetration into the stomach: (*a*) small radius of curvature, and (*b*) large radius of curvature. (*c*) Model to determine the radius of curvature of the guidewire before and after penetrate out of the stomach at point C.

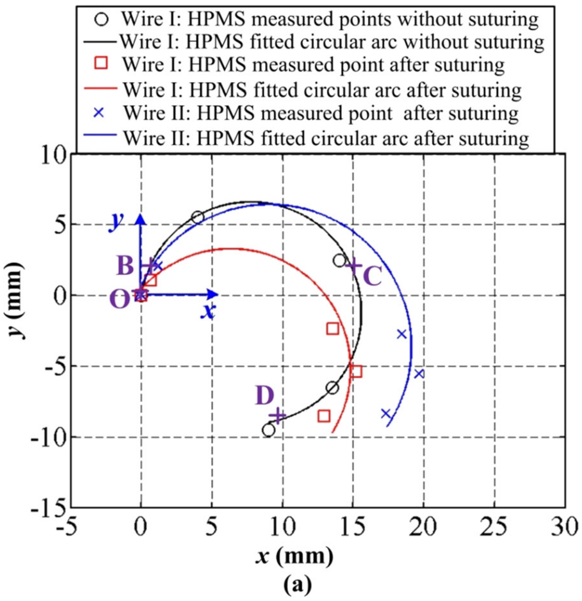

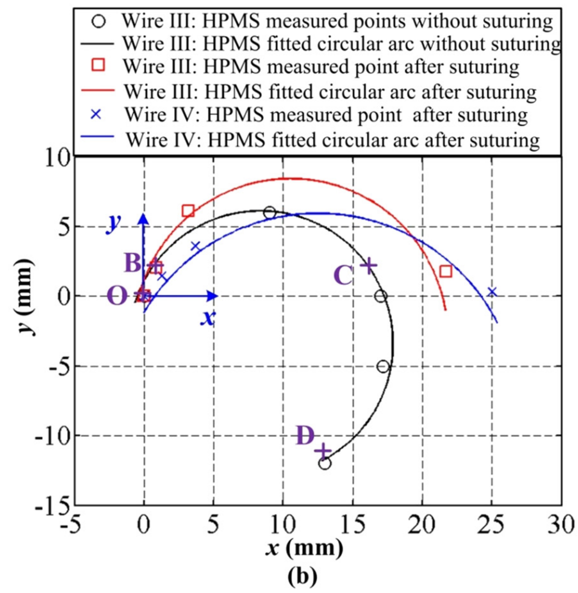

Fig. 5 HPMS measured and fitted curvatures for the four guidewires without and after suturing: (*a*) wires I and II and (*b*) wires III and IV

y-directions (marked as F_E^x and F_E^y) are the measured forces and applied at point E.

Precurved guidewire during suturing can be assumed to be a circular arc, thus this is a circular curve beam bending with F_E^x and F_E^y at point E. Castigliano's theorem [19] was adopted to estimate the displacements of point E (δ_E^x,δ_E^y) after the force is released. As the guidewire undergoes relatively large deflection, it limits the applicability of Castigliano's theorem and affects the calculated values of radius of curvature. Therefore, the calculation of the changed radius of curvature based on Castigliano's theorem can only be seen as estimation. The effect of shear stress was not considered because the guidewire during suturing has a relatively large arc length and much smaller diameter ($d = 0.69$ mm) with respect to the radius of curvature (in the 7–9 mm rage). In Fig. 4(*c*), F_E^x and F_E^y generate a moment M at point K on the guidewire and can be expressed as

$$M_k = F_E^x R(\cos\varphi - \cos\theta_E) + F_E^y R(\sin\theta_E - \sin\varphi) \tag{1}$$

The partial derivatives of M_k versus F_E^x and F_E^y are

$$\frac{\partial M_k}{\partial F_E^x} = R(\cos\varphi - \cos\theta_E), \quad \frac{\partial M_k}{\partial F_E^y} = R(\sin\theta_E - \sin\varphi) \tag{2}$$

The δ_E^x and δ_E^y can be calculated as [23]

$$\delta_E^x = \int_0^{\theta_E} \frac{M_k}{EI}\frac{\partial M_k}{\partial F_E^x} R d\varphi = \frac{1}{EI}\int_0^{\theta_E} \left[F_E^x R^3(\cos\varphi - \cos\theta_E)^2 \right. \\ \left. + F_E^y R^3(\sin\theta_E - \sin\varphi)(\cos\varphi - \cos\theta_E)\right] d\varphi \tag{3}$$

$$\delta_E^y = \int_0^{\theta} \frac{M_k}{EI}\frac{\partial M_k}{\partial F_E^y} R d\varphi = \frac{1}{EI}\int_0^{\theta_E} \left[F_E^y R^3(\sin\theta_E - \sin\varphi)^2 \right. \\ \left. + F_E^x R^3(\sin\theta_E - \sin\varphi)(\cos\varphi - \cos\theta_E)\right] d\varphi \tag{4}$$

where E is the Young's modulus (=50 GPa for NiTi) [16] and I is second moment of inertia ($=\pi d^4/64$ for the guidewire).

Based on Eqs. (3) and (4), the position of point E after penetrating out of the stomach (E_1) can be determined by δ_E^x and δ_E^y. The length of line OE_1 ($l_{\overline{OE_1}}$) can be calculated. The angle $\angle E_1O_1O$ is θ_1 and the radius of curvature of the guidewire after penetration is R_1. The relationship of θ_1 and R_1 with $l_{\widehat{OE}}$ and $l_{\overline{OE_1}}$ can be expressed as

$$R_1\theta_1 = l_{\widehat{OE}} \tag{5}$$

$$R_1 \sin(\theta_1/2) = l_{\overline{OE_1}}/2 \tag{6}$$

Using the MATLAB 7.12 (MathWorks Inc., Natick, MA) and values of $l_{\widehat{OE}}$ and $l_{\overline{OE_1}}$, θ_1 and R_1 can be calculated.

3 Results

3.1 Shape and Radius of Curvature of Guidewires. Figure 5 shows the position of four measurement points (O, B, C, and D) and three fitted circular arcs for wires I and II (Fig. 5(*a*)) and III and IV (Fig. 5(*b*)) with and without suturing. Since the only difference of wires I and II is the bevel angle, it is assumed that wires I and II without suturing have almost the same shape. Similarly,

Table 1 The radius of curvature for wires I, II, III, and IV without and after suturing

	Without suturing				After suturing		
		HPMS[a]			HPMS[a]		
	Micrometer measurement (mm)	Average (mm)	Standard deviation (mm)	Discrepancy to micrometer measurement (%)	Average (mm)	Standard deviation (mm)	Increases from without suturing (%)
Wire I	7.61	7.85	0.18	3.2	7.95	0.52	4.5
Wire II	7.93	—	—	—	10.7	0.60	34.6
Wire III	9.27	9.73	0.53	5.0	11.0	0.54	18.3
Wire IV	8.96	—	—	—	13.4	1.14	49.1

[a]Points OBCD fit to a circular arc.

without suturing, wires III and IV were also assumed to have the same shape. Table 1 summarizes the results of radii of curvature of the guidewire with and without suturing the stomach. The HPMS measured radii of curvature of wires I and III are 7.85 and 9.73 mm (only 3.2% and 5.0% difference compared to micrometer measured radii of curvature of 7.61 and 9.27 mm, respectively).

After suturing, the radii of curvature of the guidewires increase due to the suturing force induced deformation. For wires I and II with 5 deg and 10 deg bevel angle, the radii of curvature after suturing increased from 7.85 mm to 7.95 mm (4.5%) and 10.7 mm (34.6%), respectively. The sharp tip of wire I had a lower suturing force (as shown later in Fig. 6) and thus a smaller deformation. Similarly, for wires III and IV, the radius of curvature increased from 9.73 mm to 11.0 mm (18.3%) and 13.4 mm (49.1%), respectively. Generally, the lower force and less guidewire deformation enable more accurate guidewire suturing.

3.2 Precurved Guidewire Insertion Force. Figure 6 shows the measured insertion force components F_x and F_y versus time for wires I−IV while suturing the stomach. From the force curve, there exist seven phases.

(1) Deformation prior to penetration: The insertion force starts to increase when the guidewire begins to contact the inner-layer (mucosa) of the stomach and ends at the initial peak force (H), where the guidewire tip penetrates into the mucosa.
(2) Penetration into the mucosa: This phase starts from the first drop in force (H) and ends at the second drop in force (M).
(3) Penetration into the stomach outer-layer (muscularis): This phase starts from point M and ends at point N, which is the end of tissue cutting. The force then decreases suddenly.
(4) Steady-state penetration: This phase starts after the guidewire tip completely penetrates through the stomach wall and has curved toward the muscularis. The force is due to friction between the guidewire shaft and tissue.
(5) Penetration into muscularis: The insertion force increases as the guidewire tip contacts the outer surface of the muscularis.
(6) Penetrating the mucosa: This penetration ends at point Q, which is also the end of tissue cutting.
(7) Steady-state penetration: The insertion force is caused by the friction between the guidewire and two stomach wall insertion points.

Forces at H (initial insertion force), M (penetration into the stomach), Q (penetration out of the stomach) are critical to evaluate the performance of a guidewire. The force at H is required to initially fracture the tissue bonds and begin penetration [20–23]. Based on Fig. 6, the time t_M and t_Q for points M and Q can be defined. Table 2 summarizes the measured t_M and t_Q and forces at points H, M, and Q for wires I–IV. At point H, wire I generates the lowest initial insertion force (0.41 N) and wire IV has the highest initial insertion force (0.84 N). At point M, the radius of curvature has a significant effect on the insertion force. Wire I with 7.61 mm radius of curvature generates a larger forces ($F_M^x = 1.56$ N and $F_M^y = -0.18$ N) and longer t_M (6.86 s) than that of wire III with 9.27 mm radius of curvature ($F_M^x = 1.06$ N, $F_M^y = 0.04$ N, and $t_M = 5.67$ s).

To penetrate out of the stomach (point Q), both the radius of curvature and bevel angle had significant effects on the insertion forces. The guidewires with smaller radii of curvature had greater insertion forces, as shown in Fig. 6. During this period, wire I with a 5 deg bevel angle generates a lower insertion force (0.93 N) than that of wire II with 10 deg bevel angle (1.14 N). Also, wire III has 0.64 N, much lower than wire IV (0.95 N).

3.3 Precurved Guidewire. Using the forces measured at point Q (Table 2) as (F_E^x, F_E^y), the radius of curvature after penetrating the stomach at point C can be calculated. Table 3 summarizes the model calculated and HPMS measured radius of

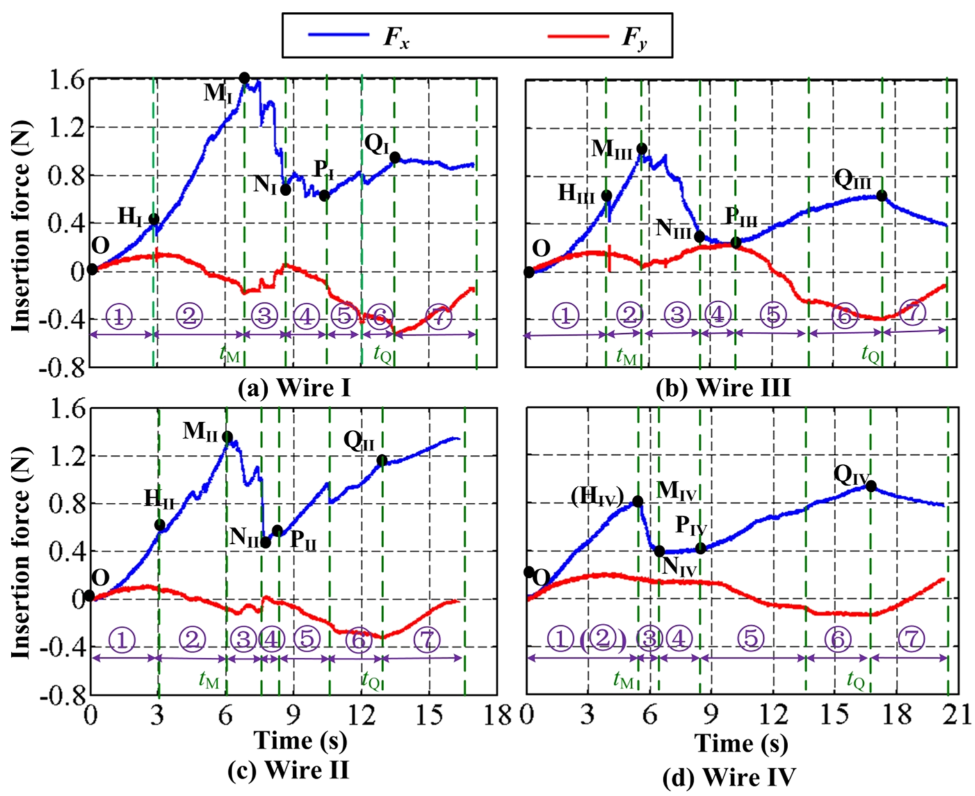

Fig. 6 Guidewire insertion forces versus time for wires I, II, III, and IV suturing into the stomach. (*a*) Wire I, (*b*) wire III, (*c*) wire II, and (*d*) Wire IV.

Table 2 Insertion forces at H, M, Q, and time t_M and t_Q in the measured forces curve for wires I, II, III, and IV

			Forces at point H (N)		Forces at point M (N)		Forces at point Q (N)	
	t_M (s)	t_Q (s)	F^x_H	F^y_H	F^y_M	F^y_M	F^x_Q	F^y_Q
Wire I	6.86	13.57	0.41	0.14	1.56	−0.18	0.93	−0.53
Wire II	6.23	13.03	0.59	0.31	1.33	−0.13	1.14	−0.33
Wire III	5.67	17.38	0.63	0.14	1.04	0.04	0.64	−0.41
Wire IV	5.34	17.61	0.84	0.21	0.84	0.21	0.95	−0.13

Table 3 Model calculated and HPMS measured radius of curvature for wires I, II, III, and IV after suturing

Radius of curvature (mm)	HPMS measurement	Model calculation	Discrepancy from HPMS measurement (%)
Wire I	7.95	7.83	−1.5
Wire II	10.67	9.73	−8.8
Wire III	10.97	10.10	−7.9
Wire IV	13.36	11.54	−13.6

curvature with discrepancies of 1.5%, 8.8%, 7.9%, and 13.6% for wires I, II, III, and IV, respectively. The good agreement demonstrates that the analytical model can be utilized to predict the trajectory of the guidewire while suturing of a stomach by using the measured insertion force as the input.

4 Discussion

This paper investigated a precurved NiTi guidewire for stomach suturing for an endoscopic obesity treatment. The HPMS was demonstrated capable of measuring the shape and radius of curvature of thin, flexible guidewires. The insertion forces were measured and their effects on the final shape of the guidewires were studied. A mathematical model, using experimentally measured insertion forces as the input, to predict the radius of curvature of the guidewire suturing of the stomach was demonstrated achievable.

Guidewires with smaller radii of curvature (wires I and II) had less change in their radius of curvature during stomach insertion. In this study, the radius of curvature of wire I is increased by only 4.5% after suturing (versus 18.3% of wire III with the same bevel angle). The same trend can also be seen on wires II (35%) and IV (49%) with 10 deg bevel angle. The guidewire with a smaller radius of curvature is structurally stiffer and more accurate for suturing. However, it is also more challenging to manufacture. Essentially, precurved NiTi guidewires with lower bevel angles and smaller radii of curvature are best configured for accurate suturing.

Guidewire suturing forces at H (initial insertion force), M (penetration into the stomach), Q (penetration out of the stomach) are critical to evaluate the performance of a guidewire. The force at H is required to initially fracture the tissue bonds and begin penetration [20–23]. The guidewires with larger bevel angle have higher initial insertion forces. The initial insertion force for wire IV with 10 deg bevel angle is 0.84 N, about 30% greater than that of wire III with 5 deg bevel angle. The initial insertion force for wire II is 0.59 N, almost 40% larger than that of wire I. Similarly, guidewires with smaller radius of curvature generate lower initial insertion forces. For example, wire I with 7.61 mm radius of curvature has 0.41 N initial insertion force, much lower than that of wire III (0.63 N). Wire II with its small radius of curvature has 0.59 N initial insertion force, about 70% of the force generated by wire IV (0.84 N). Thus, the guidewire with a sharp tip and small radius of curvature is beneficially reduces the initial insertion force for suturing.

To penetrate into the stomach (point M), the radius of curvature has a significant effect on the insertion force. Wire I with 7.61 mm radius of curvature generates a larger forces and longer time than that of wire III with 9.27 mm radius of curvature. The reasons can be explained in Figs. 4(*a*) and 4(*b*). During the guidewire insertion, the stomach was deflected. Given the same amount of stomach deflection, the guidewire with a small radius of curvature needs a longer time to penetrate into the stomach. Also, the guidewires with smaller radii of curvature have higher stiffness, which generate greater force to penetrate into the stomach, as shown in Fig. 4(*b*). This trend was observed in wires I and III and wires II and IV, respectively. As to the effects of the needle tip bevel angle, although wires I and III have sharper tips than their counterparts, the force to penetrate into the stomach was slightly larger than that of wires II and IV. The reason for this is likely because the radius of curvature has a more significant effect on the insertion force than the bevel angle to penetrate into the stomach. Furthermore, the guidewire with a small bevel angle has a corresponding larger bevel length, which contacts the soft tissue more, and thus generates a greater insertion force, requiring a longer time to penetrate through the stomach.

After the guidewire penetrates into the stomach, the forces in *x*- and *y*-directions both decrease without new tissue cutting, and only friction force is applied on the guidewire shaft in contact with the stomach wall, as shown in Fig. 6. During this period, wires I, II, and III had relatively large variations in insertion force due to the stomach dragged by the motion of the guidewire. Wire IV had the least deflection and less force variation.

To penetrate out of the stomach (point Q), both the radius of curvature and bevel angle had significant effects on the insertion forces. The guidewires with smaller radii of curvature had greater insertion forces. The guidewire with smaller radius of curvature deflects away from the *x*-direction and requires a higher force in the *x*-direction to penetrate out of the stomach. The guidewires with smaller bevel angle generates lower insertion forces, as observed in wires I and III. This can be explained as guidewire with a shaper tip generates lower insertion force for soft tissue insertion and cutting [22,23]. The greater forces in wires II and IV pushed the guidewire away from its original shape and generated larger deflections, thus increasing the radius of curvature simultaneously more than that of wires I and III when penetrating out of the stomach. Overall, the guidewire with small bevel angle and large radius of curvature reduced the insertion force and enabled accurate precurved guidewire suturing.

The developed analytical model can predict the trajectory of the guidewire suturing of a stomach by using the measured insertion force as the input. The model calculated radii of curvatures for wires I–IV, which are all smaller than the HPMS measured values. One of the reasons for such a trend can be explained by the boundary condition set at point O. In Fig. 4(*c*), point O is fully constrained (fixed), while in the suturing procedure, the guidewire slides along the needle tube at point O as in Fig. 1. The overconstraint at O in the model will lower the calculated radius of curvature. Overall, the model predicted radius of curvature matched well with the HPMS measurements.

Knowing the behavior of precurved guidewire stomach suturing and developing a model to determine the shape of the guidewire during suturing based on measured insertion forces are necessary to the foundation of real-time prediction and visualization of guidewire suturing path. To accurately predict the shape of the precurved guidewire during suturing, a more accurate mathematical model based on nonlinear theory will be developed in the future work. Results in this research also enable the optimal design of new precurved guidewires to minimize insertion forces and increase the accuracy of guidewire suturing procedures.

Acknowledgment

This research work was sponsored by the National Natural Science Foundation of China (No. 51105333) and National Science Foundation (NSF) Award CMMI#0825795.

References

[1] Kang, H., and Wen, J., 2002, "Robotic Knot Tying in Minimally Invasive Surgeries," Proceedings of the IEEE/RSJ International Conference on Intelligent Robots and Systems, IROS 2002, pp. 1421–1426.

[2] Ishikawa, S., Kawasaki, A., Neya, K., Abe, K., Suzuki, H., Kadowaku, S., Nakamura, K., and Ueda, K., 2008, "Surgery for Infective Endocarditis: Determinate Factors in the Outcome," J. Cardiovasc. Surg., **49**(4), pp. 545–548.

[3] LeDuc, M., Payandeh, S., and Dill, J., 2003, "Toward Modeling of a Suturing Task," Graphics Interface, 3, pp. 273–279.

[4] Xu, K., Zhao, J. R., Geiger, K., Shih, A. J., and Zheng, M. H., 2011, "Design of an Endoscopic Stitching Device for Surgical Obesity Treatment Using a N.O.T.E.S Approach," Proceedings of the IEEE/RSJ International Conference on Intelligent Robots and Systems, IROS 2011, San Francisco, CA, Sept. 25–30, pp. 961–966.

[5] Dubrowski, A., Sidu, R., Park, J., and Carnahan, H., 2005, "Quantification of Motion Characteristics and Forces Applied to Tissues During Suturing," Am. J. Surg., **190**(1), pp. 131–136.

[6] Yang, Y., Xu, C. L., Deng, S. J., and Xiao, J. J., 2012, "Insertion Force in Manual and Robotic Corneal Suturing," Int. J. Med. Rob. Comput. Assist. Surg., **8**(1), pp. 25–33.

[7] Capek, L., Jacquet, E., Dzan, L., and Simunek, A., 2012, "The Analysis of Forces Needed for the Suturing of Elliptical Skin Wounds," Med. Biol. Eng. Comput., **50**(2), pp. 193–198.

[8] Jackson, R. C., and Cavusoglu, M. C., 2003, "Modeling of Needle–Tissue Interaction Forces During Surgical Suturing," Proceedings of the 2003 IEEE International Conference on Robotics and Automation, St. Paul, MN, May 14–18, pp. 2068–2073.

[9] Glozman, D., and Shoham, M., 2007, "Image-Guided Robotic Flexible Needle Steering," IEEE Trans. Rob., **23**(3), pp. 459–467.

[10] Wedlick, T. R., and Okamura, A. M., 2009, "Characterization of Pre-Curved Needles for Steering in Tissue," Proceedings of the IEEE International Conference of the Engineering in Medicine and Biology Society, Minneapolis, MN, Sept. 3–6, pp. 1200–1203.

[11] Okazawa, S., Ebrahimi, R., Chuang, J., Salcudean, S. E., and Rohling, R., 2005, "Hand-Held Steerable Needle Device," IEEE/ASME Trans. Mech., **10**(3), pp. 285–296

[12] Majewicz, A., Marra, S. P., van Vledder, M. G., Lin, M. D., Choti, M. A., Song, D. Y., and Okamura, A. M., 2012, "Behavior of Tip-Steerable Needles in Ex Vivo and In Vivo Tissue," IEEE Trans. Biomed. Eng., **59**(10), pp. 2705–2715.

[13] Chen, R. K., Wang, Y. C., Tai, B. L., and Shih, A. J., 2013, "The Haptic Position Measurement System for Position and Shape Measurement of Soft or Compliant Objects Based on Magnetic Tracking System," Manuf. Lett., **1**(1), pp. 17–20.

[14] Raab, F. H., Blood, E. B., Steiner, T. O., and Jons, H. R., 1979, "The Magnetic Position and Orientation Tracking System," IEEE Trans. Aerosp. Electron. Syst., **15**(5), pp. 709–718.

[15] Kolker, A. R., Brown, D. J., Redstone, J. S., Scarpinato, V. W., and Wallack, W. K., 2005, "Multilayer Reconstruction of Abdominal Wall Defects With Acellular Dermal Allograft (AlloDerm) and Component Separation," Ann. Plast. Surg., **55**(1), pp. 36–41.

[16] Wang, Y. C., Spangler, C., Tai, B. L., and Shih, A. J., 2013, "Positional Accuracy and Transmitter Orientation of the 3D Electromagnetic Tracking System," Meas. Sci. Technol., **24**(10), p. 105105.

[17] Nemat-Nassera, S., and Guo, W. G., 2006, "Superelastic and Cyclic Response of NiTi SMA at Various Strain Rates and Temperatures," Mech. Mater., **38**(5), pp. 463–474.

[18] Wang, Y. C., Tai, B. L., Van, L. M., and Shih, A. J., 2012, "Grinding the Sharp Tip in Thin NiTi and Stainless Steel Wires," Int. J. Mach. Tools Manuf., **62**, pp. 53–60.

[19] Timoshenko, S., and Goodier, J. N., 1951, *Theory of Elasticity*, McGraw-Hill Book Company, Inc., New York.

[20] Okamura, A. M., Simone, C., and O' Leary, M. F., 2004, "Force Modeling for Needle Insertion Into Soft Tissue," IEEE Trans. Biomed. Eng., **51**(10), pp. 1707–1716.

[21] Moore, J. Z., Malukhin, K., Shih, A. J., and Ehmann, K. F., 2011, "Hollow Needle Tissue Insertion Force Model," CIRP Ann. Manuf. Technol., **60**(1), pp. 157–160.

[22] Wang, Y. C., Tai, B. L., Chen, R. K., and Shih, A. J., 2013, "The Needle With Lancet Point—Geometry for Needle Tip Grinding and Tissue Insertion Force," ASME J. Manuf. Sci. E, **135**(4), p. 041010.

[23] Abolhassani, N., Patel, R., and Moallem, M., 2007, "Needle Insertion Into Soft Tissue: A Survey," Med. Eng. Phys., **29**(4), pp. 413–431.